Title
Thin High-Impedance Metamaterial Substrate and its Use in Low Profile Antennas Suitable for System Integration

ISBN
978-1-4244-4475-5

Authors
Vallecchi, A
Capolino, F

Publication Date
2009-05-01

DOI
10.1109/ectc.2009.5074100

Thin High-Impedance Metamaterial Substrate and its Use in Low Profile Antennas Suitable for System Integration

A. Vallecchi and F. Capolino
Department of Electrical Engineering and Computer Science, University of California, Irvine, CA 92697-2625
f.capolino@uci.edu

Abstract

We present a metamaterial substrate designed to act as a high impedance thin slab that can be used to integrated low-profile (subwavelength thickness) antennas in components or packages. A transverse equivalent network (TEN) model accurately describing the reflection properties of the impedance substrate is also provided to facilitate its design. Then, we develop a low profile planar antenna consisting of a printed dipole located on top of the parallel metamaterial substrate. The high impedance of the substrate permits to locate the metallic dipole very close to the substrate itself without inhibition of the dipole radiation. The substrate prevents radiation from traveling across the substrate, resulting in a low profile antenna with high efficiency, even though the antenna system is integrated on top of a lossy structure. Two possible feed structures for the dipole over the impedance surface are considered, and simulation data are presented to illustrate their respective performance.

Introduction

We have seen a growing interest in installing small antennas in packaging and devices. This usually imposes several critical challenges because the antenna performance (e.g., bandwidth and efficiency) degrades when reducing its size. Frequently, the antenna has to be mounted near a high loss dielectric material or near a ground plane. The high loss material would lower the efficiency of the antenna, whereas the presence of the ground plane would "short circuit" the antenna radiation, again resulting in low efficiency. Therefore, it is highly desirable to develop solutions that would limit these two impairing effects. One possibility is the introduction of a special antenna substrate which is very thin and shields the antenna field from lossy structures and from having reflected fields that do not cancel the direct radiation.

On-chip antennas have already been designed using multiple metal layers [1]-[4], though in most designs radiation is not set off (orthogonal to) the chip (as instead proposed in this study). Also, these antennas radiate mainly in the lossy substrate, resulting in extremely low antenna gains (i.e., low efficiency) at millimeter waves. The reason is the very high dielectric permittivity ($\varepsilon_r = 11.7$) of the silicon substrate, that would attract most of the power radiated by an antenna. For example, the 140-GHz on-chip antenna implemented in 65nm CMOS technology by [3] has a gain of only -25dB.

Metamaterials are artificial engineered materials synthesized by embedding specific inclusions, for example, periodic structures, in the host media [5], [6]. Some of these materials exhibit either negative permittivity or negative permeability, but other extreme properties like high permeability or very low permittivity can be engineered, which are those needed to design a high impedance substrate or surface.

High impedance surfaces (HIS) have been initially realized by using the so called "mushroom" structure [7] that however needs a ground plane and metallic vias long enough to guarantee inductive energy accumulation in the substrate itself. Other HIS have been designed without vias but they still require a continuous ground plane. Our structure made of pairs of tightly coupled layers of arrayed printed geometries possesses more general properties and the constituent cells are in general smaller than those previously reported in the literature. It can be designed with or without the support of a continuous ground plane, and one or more layers depending on the required properties, could be used. Other existing metamaterials exhibiting artificial magnetism are based on conducting split ring resonators [5], [6] that however cannot be assembled in planar technology thus rendering their use difficult in a variety of applications, like the one discussed herein for low profile antennas. Conversely, the metamaterial we propose is fabricated entirely in planar technology [8]-[12]. And one of its advantages is that it does not require metallic vias between its layers. Contrarily to the mushroom-like structure a large enough inductance is obtained by shrinking the central part of the dogbones, even in very thin layers. This kind of metamaterial is based on arrayed pairs of tightly coupled planar conductors with proper shape (like dogbones, Jerusalem crosses, tripoles, etc.) that feature both a magnetic resonance (antisymmetric mode) and an electric resonance (symmetric mode) that can be properly tuned to the desired frequency by adjusting the length and shape of the pair [10]-[12].

In this work we focus on two important technological novelties. First we present a novel metamaterial substrate designed to act as a high impedance thin slab. Then, we will show the design of a low profile antenna that consists of a printed dipole located on top of this parallel metamaterial substrate. The high impedance of the substrate permits to locate the metallic dipole very close to the substrate itself without inhibition of the dipole radiation. Furthermore, the substrate inhibits radiation to travel across, resulting in a low profile antenna with high efficiency, even though the antenna system (comprising the dipole and thin metamaterial substrate) is integrated on top of a lossy structure.

We provide a solid theoretical background for the design of the high impedance metamaterial substrate, and to facilitate the design of such planar structures we also develop an equivalent circuit.

Indeed, the proposed low profile antenna design is suitable for integration in supporting platforms like metallic structures or chips where also active components could be assembled, and can be fabricated in CMOS technology. It is also suitable for wearable antennas that have the constraints of being flat and simple to be realized n thin flexible substrates. Properly scaled, it can be designed for a large

978-1-4244-4476-2/09/$25.00 ©2009 IEEE

variety of frequency bands from microwaves to millimeter waves.

Numerical simulations of the low profile antenna (conducting dipole printed on the metamaterial substrate) with two different feeding structures are presented to show the effectiveness of our design. Despite the overall small thickness, compared to the wavelength, our low profile antenna exhibits good matching on a significant bandwidth (small bandwidth is usually a serious constraint when using metamaterials) and a dipole-like radiation pattern though with a significant increase of directivity. Fabrication and testing of a prototype will be presented during the oral presentation.

Metamaterial in Planar Technology

The planar metamaterial is made of arrayed pairs of metallic conductors with a dogbone shape (Fig. 1). Because of the tight coupling of the two conductors, two working regimes can be excited: the *symmetric* and the *antisymmetric* current mode distributions. The antisymmetric mode, also called transmission line (TL) mode, has been associated to artificial magnetism, since each antisymmetric current forms a loop that can be associated to an equivalent magnetic dipole oriented along the *y*-direction [11].

A layer of arrayed pairs exhibits complex transmission and reflection spectra because of the interplay of the two kinds of resonant modes that can be excited. It has been shown that a stack of layers may exhibit a negative index of refraction and thus it supports a backward-wave travelling across them [11]. Furthermore, we show here that the characteristic impedance of each layer can be engineered to provide a high impedance material.

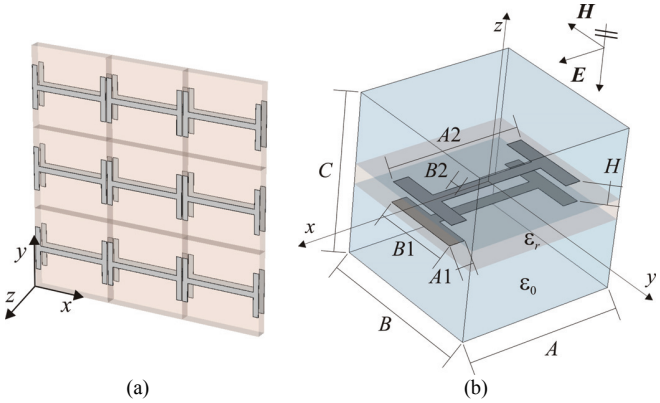

Fig. 1 (a) Perspective view of a layer of the metamaterial formed by a periodic arrangement of tightly coupled pairs of dogbone-shaped conductors printed on a dielectric substrate. (b) Metamaterial elemental particle (unit cell) with geometrical parameters quoted. The polarization of the incident electric field is along the *x*-direction. The anti-symmetric mode of the particle creates a magnetic dipole along the *y*-direction.

The TL model consists in replacing the layer of arrayed conductor pairs by the equivalent 2-ports network shown in Fig. 2, made by lumped physically realizable circuital elements. Neglecting losses (in these initial simulations) both in the conductors and the dielectric substrate, the impedances of the equivalent X-network are only made by *L*-*C* elements that take into account both the electric and magnetic resonances characterizing the metamaterial response. As shown in Fig. 2, the magnetic resonance is described by a parallel *LC* resonator Z_A, whereas the electric resonance, as the usual stop band of capacitive FSSs, is described by a series *LC* resonator Z_B.

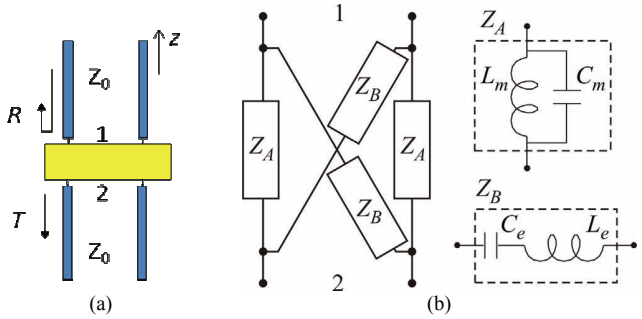

Fig. 2 Equivalent network for the metamaterial layer made of arrayed pairs of dogbone-shaped conductors and its inclusion in a TL model.

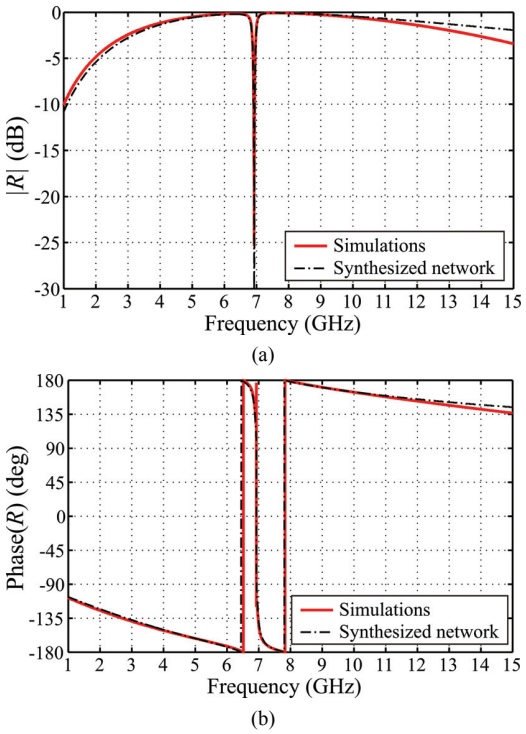

Fig. 3 Reflection coefficient vs. frequency for a layer of dogbones pairs: (a) magnitude; (b) phase. The *magnetic* resonance is at $f_m \approx 6.9$ GHz, whereas the *electric* resonance is at $f_e \approx 7.3$ GHz. Data from a numerical analysis are compared with those from our proposed equivalent network model.

As an example, we consider the response of a layer of dogbones pairs printed on a dielectric substrate with $\varepsilon_r = 2.2$ (e.g., RT Duroid 5880). The various geometrical parameters characterizing the unit cell of the considered metamaterial (cf. Fig. 1 (b)) are as follows (in mm): $A = 7.5$, $B = 7.5$, $A1 = 0.5$, $B1 = 4$, $A2 = 7.4$, $B2 = 0.5$, $H = 1.0$. The dimension of the unit cell along the *z*-direction is $C = 8.0$ mm, and therefore ports are defined at $z = \pm 4$mm. The magnitude and phase of the reflection coefficient *R* in Fig. 3 predicted by the synthesized TL and X-network are in good agreement with those obtained numerically with the commercial software CST Microwave

Studio. The electric and magnetic frequencies are f_m = 6.89 GHz, and f_e = 7.30 GHz, respectively.

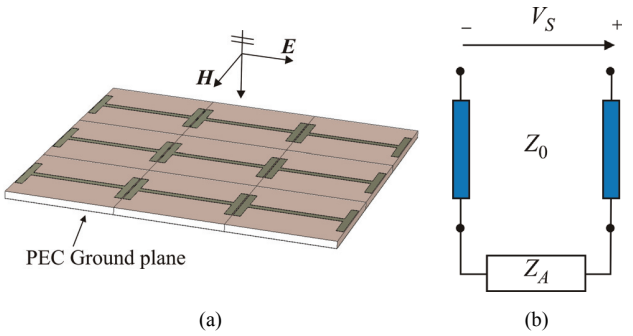

Fig. 4 (a) RIS substrate composed of a periodic array of dogbone-shaped conductors printed on a PEC-backed dielectric material and illuminated by a plane wave. (b) Circuit approach representation of the RIS.

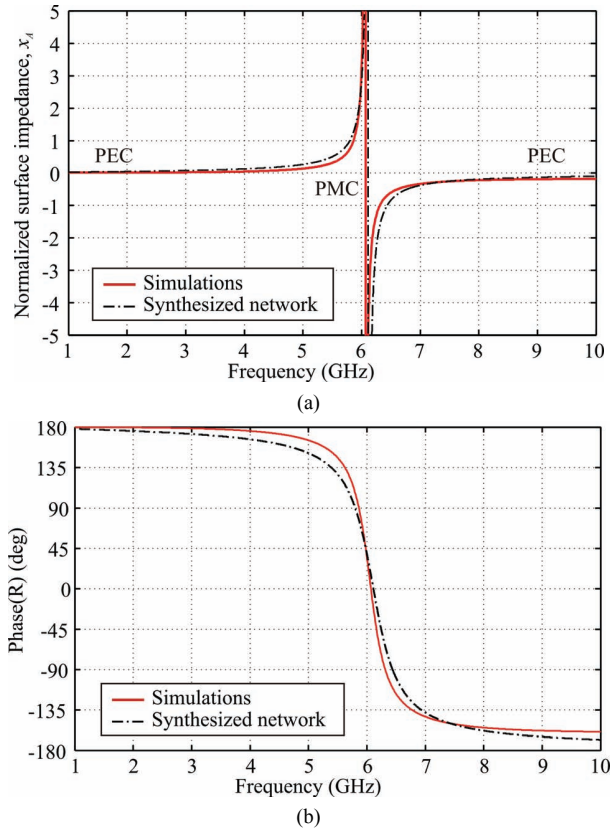

Fig. 5 Characteristics at normal incidence of an RIS substrate printed on a PEC-backed dielectric substrate with thickness H = 1.6 mm and permittivity $\varepsilon_r = 2.2$ with tan δ = 0.0009. The dimensions of the unit cell of the considered periodic material (cf. Fig. 2) are as follows (in mm): A = 8, B = 8, $A1$ = 0.5, $B1$ = 4, $A2$ = 7.8, $B2$ = 0.5. Results obtained through the equivalent circuit approach (dashed-dotted lines) are compared with data from full-wave simulations (red lines). (a) Normalized surface impedance, and (b) reflection coefficient phase.

Low Profile Dipole on a Reactive Impedance Surface

The equivalent circuit developed above can be applied to the design of a low profile antenna consisting of a dipole located on top of a reactive impedance surface (RIS) [14]. The high impedance exhibited by the RIS permits to locate the metallic dipole very close to the surface itself without inhibition of the dipole radiation. Furthermore, the substrate prevents radiation from travelling across, resulting in a low profile antenna with high efficiency, even though the antenna system (comprising the dipole and thin metamaterial substrate) is integrated on top of a lossy structure.

An RIS structure composed of a periodic array of dogbones printed on a PEC-backed dielectric substrate (e.g., RT Duroid 5880, with losses tan δ = 0.0009) with thickness H = 1.6 mm and permittivity $\varepsilon_r = 2.2$ is introduced (Fig. 4(a)). The geometrical parameters characterizing the unit cell of the considered periodic material (cf. Fig. 2) are as follows (in mm): A = 8, B = 8, $A1$ = 0.5, $B1$ = 4, $A2$ = 7.8, $B2$ = 0.5.

To facilitate the design procedure, a simple and yet very accurate circuit model for this structure is derived starting from the equivalent network developed for a metamaterial layer of dogbone pairs with dielectric substrate thickness twice that of the RIS ($2H$). In fact, in the hypothesis of illumination by two normally incident plane waves with antisymmetric polarization of the electric field, the original metamaterial layer can be split in two identical parts backed by a PEC plane, each of which corresponds to the considered a RIS. Accordingly, the structure can be modelled using a TL approach as shown in Fig. 4(b).

The normalized surface reactance x_A ($jx_A = Z_A / Z_0$) of the RIS as a function of frequency is plotted in Fig. 5(a). Both data obtained from full-wave simulations (CST Microwave Studio) and the equivalent circuit are displayed, and the two set of results are in satisfactorily good agreement. Moreover, the phase of the reflection coefficient R of the RIS at normal incidence as deduced from the circuit representation ($R = (Z_A - Z_0)/(Z_A + Z_0)$) and calculated by CST are shown in Fig. 5(b), and again an excellent agreement is observed. As apparent, this structure, depending upon the operating frequency, can behave as a capacitive or inductive RIS. The reactance is inductive at frequencies below resonance, open circuit at the resonance (behaving as an artificial magnetic conductor (AMC) surface) and capacitive above the resonant frequency. At frequencies much lower than the resonant frequency the RIS shows low impedance and acts as a PEC surface and at the resonance the reactance goes to infinity and the RIS behaves as a AMC.

We now examine the performance of a dipole over the RIS considered above; the geometry of the dipole over the finite-size RIS is shown in Fig. 6. The finite-size RIS is composed of a 7×8 array of dogbone-shaped conductors. The dipole antenna has length 21.35 mm and width-to-length ratio of about 0.04. The dipole is excited using a delta-gap source at the centre (we just want to show the feasibility of this geometry, without worrying about the actual shape that also depends on the particular application). The height of the dipole above the RIS is 1.6 mm and thus the total thickness of the antenna (including the dipole and the substrate) is 3.2 mm. The operating frequency of the dipole in free space is 6.25 GHz at which frequency its length is 0.45 λ.

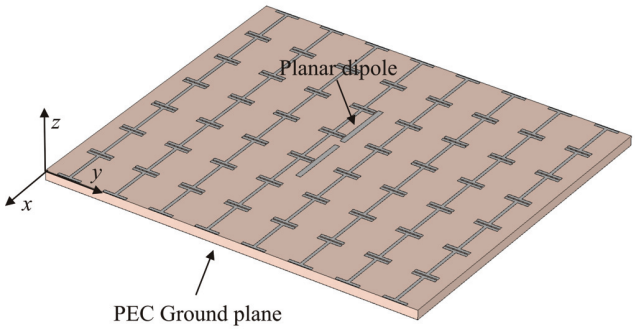

Fig. 6 Dipole antenna over a finite RIS made of a 7x8 array of dogbone-shaped conductors with the dimensions specified in Fig. 5. The total thickness is 3.2 mm, which is equal to λ/17 at the operating frequency.

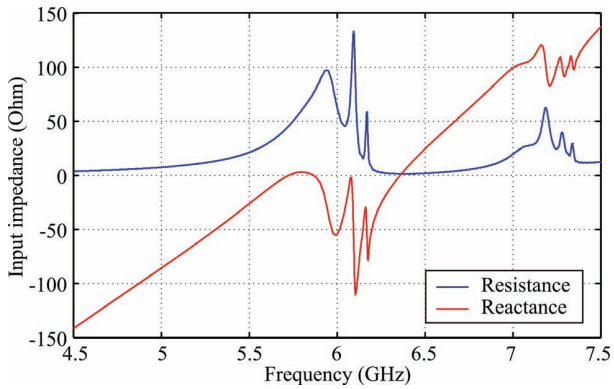

Fig. 7 (a) Input resistance and reactance, and (b) return loss of the dipole antenna on the RIS substrate.

The input impedance and the radiation patterns of the antenna are obtained using CST MS and are shown in Fig. 7 and Fig. 8, respectively. As demonstrated in Fig. 5(a), the RIS has a resonant frequency of about 6.1 GHz at which it acts like an AMC. Below this resonance the RIS is inductive. Because the dipole resonates at 6.25 GHz, below this frequency the dipole is capacitive. As a result the operating frequency of the dipole over the RIS is at f = 5.7 GHz, rather below the free-space operating frequency 6.25 GHz. At this frequency the dipole length is about 0.41 λ. Fig. 7 (b) shows the return loss of the dipole over the RIS, and it is seen that an operating bandwidth of about 6% is achieved as a result of a sufficient thickness of the RIS. Referring to Fig. 8, the radiation pattern of the dipole over the RIS at f = 5.7 GHz shows a remarkably good front-to-back ratio of about 22.5 dB. Simulation results also show a gain of 8.6 dBi and a high radiation efficiency of 96% (taking into account both ohmic (Cu metal) and dielectric losses).

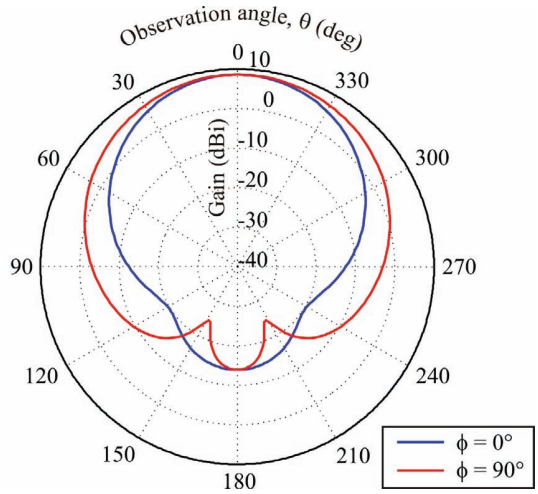

Fig. 8 Radiation patterns of the dipole antenna over the RIS substrate (Fig. 6) at 5.7 GHz in the principal planes of radiation ϕ = 0° (E-plane) and ϕ = 90° (H-plane).

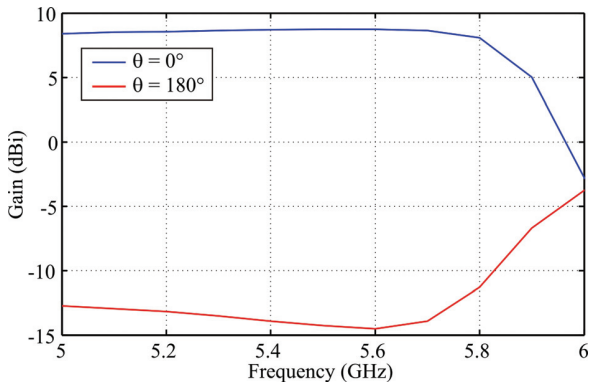

Fig. 9 Boresight gain and back radiation of the dipole antenna over the RIS substrate (Fig. 6) vs. frequency.

In practice, several different feed structures can be used to excite the dipole placed over the RIS. In the following, we consider two possible different feed arrangements. In the first configuration, shown in Fig. 10, the dipole is fed by a coaxial cable protruding through a hole in the RIS substrate. One of the dipole arms is connected to the central conductor of the coaxial cable, whereas the other arm is soldered to the outer conductor. As in Fig. 6, the finite-size RIS is composed of a 7×8 array of dogbone-shaped conductors with the same dimensions and grounded dielectric substrate characteristics of that considered previously in Fig. 5. Impedance matching of this antenna is achieved when the dipole antenna has a length of 20.85 mm and width-to-length ratio equal to 0.04. The input impedance and the radiation patterns of the antenna as obtained by using CST MS are shown in Fig. 11 and Fig. 12, respectively. The input impedance and return loss exhibit a dual resonance characteristic which may be the result of

direct radiation or coupling of the coaxial cable to some leaky modes supported by the RIS.

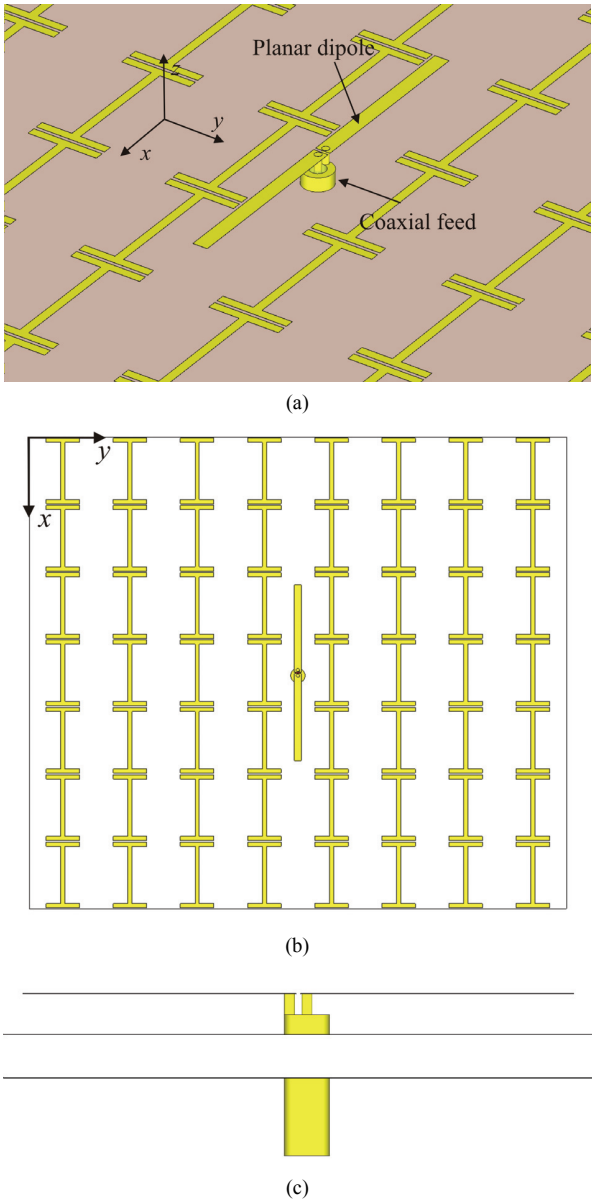

Fig. 10 Dipole antenna fed by a coaxial cable over the RIS substrate. As in Fig. 6, the RIS is a 7x8 finite array of dogbone-shaped conductors with the same dimensions and grounded dielectric substrate characteristics of that considered in Fig. 5. (a) Perspective, (b) top, and (c) lateral views of the antenna. The total thickness is 3.2 mm, which is equal to λ/17 at the operating frequency.

Indeed, since the coaxial cable is not a balanced feed, common mode currents flowing on the outer shield can cause the coaxial line to radiate in addition to the dipole itself, and the radiation pattern may be asymmetrically distorted. As a consequence, though the impedance bandwidth of the dipole fed by a coaxial cable is noticeably larger that of the ideal case of Fig. 7 (about 12.7%), it appears from the pattern plots (Fig. 12) that maximum gain is squinted off the boresight (about 12° at 5.8 GHz, the frequency considered in the plots from Fig. 12, and the maximum gain is 7.4 dBi). Moreover, beam squinting off boresight is frequency-dependent, and the

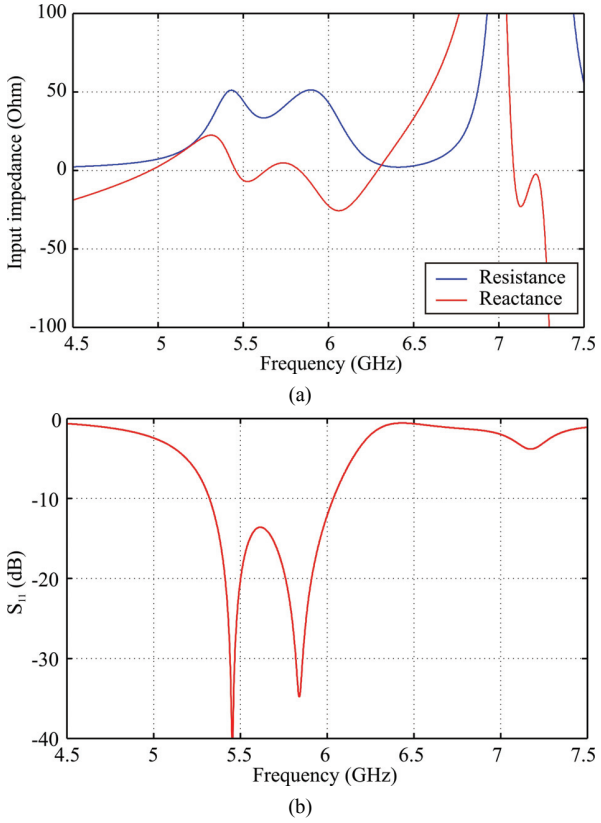

Fig. 11 Input impedance of the dipole antenna over the RIS substrate fed by a coaxial cable: (a) input resistance and reactance and (b) return loss.

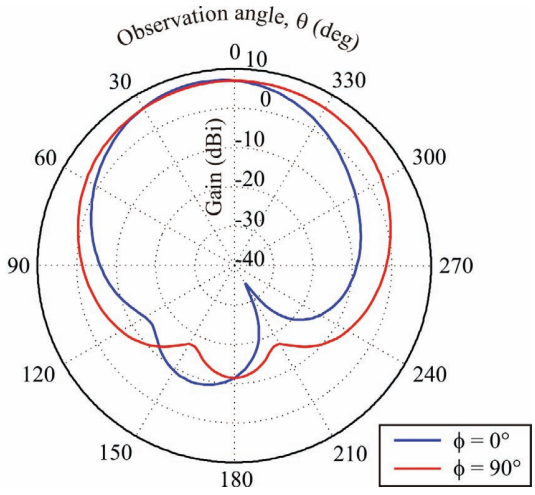

Fig. 12 Radiation patterns of the dipole antenna over the RIS substrate shown in Fig. 10 at 5.8 GHz in the principal planes of radiation $\phi = 0°$ (E-plane) and $\phi = 90°$ (H-plane).

beam pointing direction rapidly moves with frequency, so that the limiting factor in this configuration is the gain bandwidth instead of the impedance bandwidth. This is clearly illustrated from Fig. 13, where the boresight gain for the dipole configuration of Fig. 10 is plotted against frequency, that shows that, differently from the analogous results displayed in Fig. 9 for the dipole without feed, the gain

rapidly drops below 0 dB as the frequency moves away from 5.7 GHz.

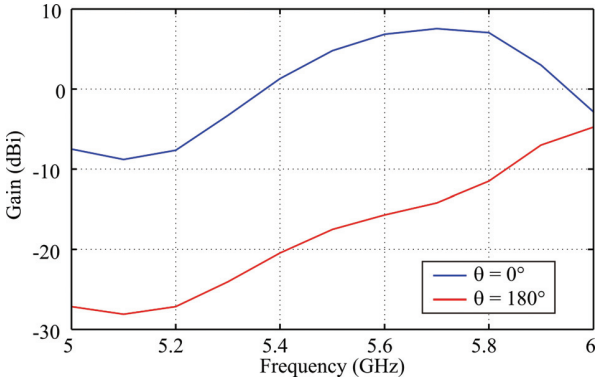

Fig. 13 Boresight gain and back radiation vs. frequency for the dipole antenna over the RIS substrate shown in Fig. 10.

In the second feeding configuration, shown in Fig. 14, the dipole is fed by a bifilar line, running on the same layer of the dipole, whose two conductors are directly connected to the dipole arms. Here, we have adopted a reduced size RIS composed of a 5×6 array of dogbone-shaped conductors on the grounded dielectric. The dimensions of the unit cell of the periodic surface and the characteristics of the supporting dielectric substrate are the same as those of the RIS used in the previous examples, which are summarized in the caption of Fig. 5. Impedance matching of this antenna is achieved when the dipole antenna has a length of 23.4 mm and width-to-length ratio equal to 0.085. The input impedance and the radiation patterns of this antenna calculated by CST MS are shown in Fig. 15 and Fig. 16, respectively. The input impedance and return loss are shown in Fig. 17. The impedance bandwidth is 4.2%, somewhat smaller that the ideal case of Figs. 6 and 7. In this case this feed is completely balanced and that's probably why there is a significant difference compared to the coaxial cable feed case. The gain at 5.7 GHz is about 8 dBi and is more uniform versus frequency than the previous case in Fig. 13.

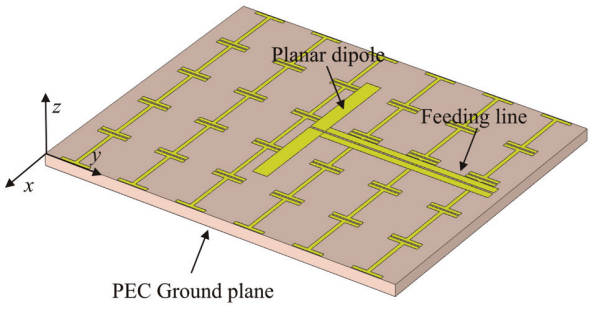

(a)

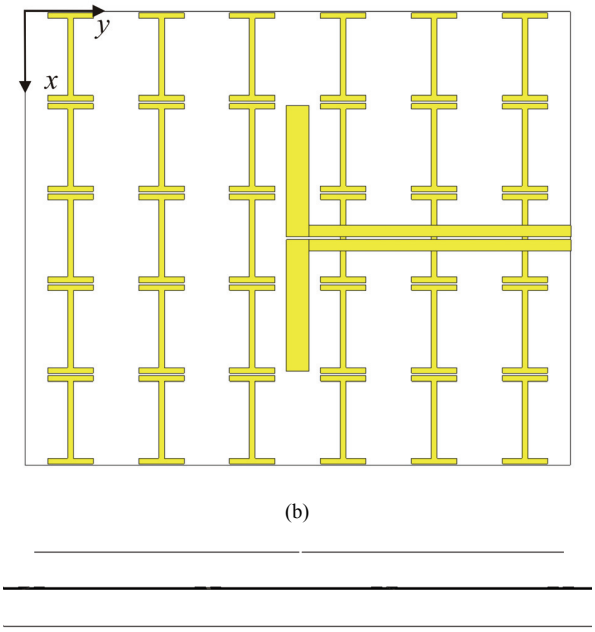

(b)

(c)

Fig. 14 Dipole antenna fed by a bifilar line over the RIS substrate. The RIS consists of 5x6 finite array of dogbone-shaped conductors with the same dimensions and dielectric substrate characteristics of that considered previously in Fig. 5. (a) Perspective, (b) top, and (c) lateral views of the antenna. The total thickness is 3.2 mm, which is equal to λ/17 at the operating frequency.

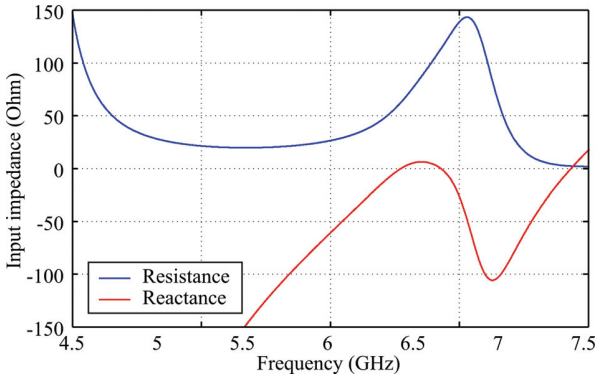

(a)

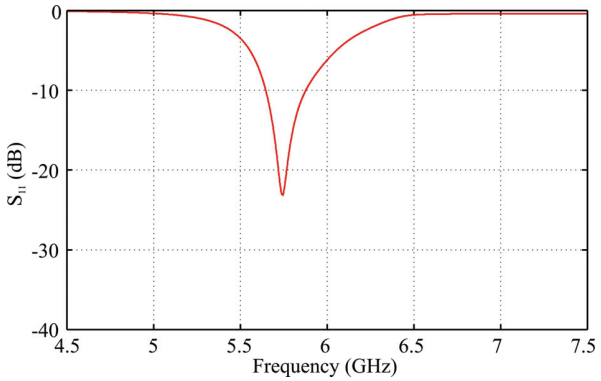

(b)

Fig. 15 Input impedance of the dipole antenna over the RIS substrate shown in Fig. 14: (a) input resistance and reactance and (b) return loss.

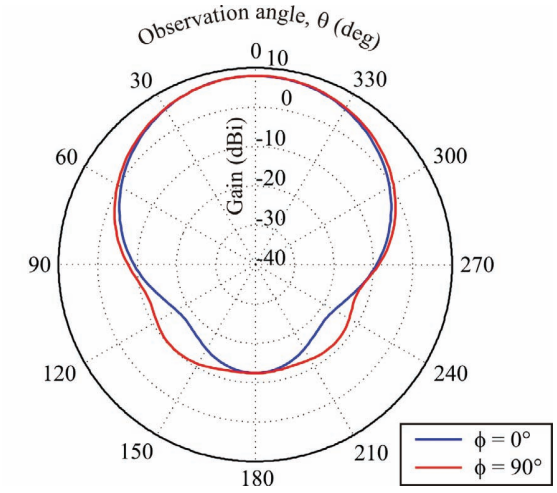

Fig. 16 Radiation patterns of the dipole antenna over the RIS substrate shown in Fig. 14 at 5.7 GHz in the principal planes of radiation $\phi = 0°$ and $\phi = 90°$.

Conclusions

In this work we have focused on two important technological novelties aiming at designing antennas that can be integrated into complex systems. First we have introduced a novel metamaterial substrate designed to act as a high impedance slab. Then, we have shown the design of a low profile antenna consisting of a printed dipole located on top of this metamaterial substrate. The high impedance of the substrate permits to locate the metallic dipole very close (subwavelength distance) to the substrate itself without inhibition of the dipole radiation and its efficiency. Furthermore the substrate inhibits radiation to travel across, resulting in a low profile antenna with high efficiency, even though the antenna system is integrated on top of a lossy structure. The behavior of two realistic feeding structures have also been examined.

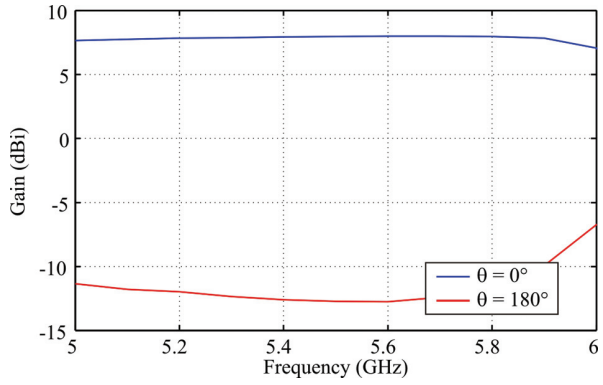

Fig. 17 Boresight gain and back radiation vs. frequency for the dipole antenna over the RIS substrate shown in Fig. 14.

References

1. M. Sun, Y.P. Zhang, "100GHz Quasi-Yagi Uda Antenna in Silicon Technology," *IEEE Electron Dev. Lett.,* vol. 28, p. 455, 2007.
2. S-S. Hsu, K-C Wei, C-Y. Hsu, and H. Ru-Chang, "A 60GHz Millimeter CPW-Fed Yagi Antenna Fabricated by Using 0.18-μm CMOS Technology," *IEEE Electron Device Lett.,* vol. 29, p. 625, 2008.
3. S. T. Nicolson, A. Tomkins, K. W. Tang, A. Cathelin, D. Belot, and S. P. Voinigescu, "A 1.2V, 140GHz Receiver with on-Die Antenna in 65nm CMOS," *IEEE Radio Freq. Integr. Circ. Symp., p. 229, 2008*.
4. P.H. Park, "An On-Chip Dipole Antenna for Millimeter-Wave transmitter," *IEEE Radio Freq. Integr. Circ. Symp.,* p. 629, 2008.
5. J. B. Pendry, A. J. Holden, D. J. Robbins, and W. J. Stewart, "Magnetism from conductors and enhanced nonlinear phenomena," *IEEE Trans. Microw. Theory Tech.*, vol. 47, no. 11, pp. 2075–2084, Nov. 1999.
6. D. R. Smith, W. J. Padilla, D. C. Vier, S. C. Nemat-Nasser, and S. Schultz, "Composite medium with simultaneously negative permeability and permittivity," *Phys. Rev. Lett*., vol. 84, pp. 4184–4187, 2000.
7. D. Sievenpiper, L. Zhang, R. F. Jimene Broas, N. G. Alexopolous, E. Yablonovitch, "High-Impedance Electromagnetic Surfaces with a Forbidden Frequency Band" *IEEE Trans. Microwave Theory Techn.*, Vol. 47, No. 11, pp. 2059-2074, Nov. 1999.
8. V. M. Shalaev, W. Cai, U. K. Chettiar, H. Yuan, A. K. Sarychev, V. P. Drachev, and A. V. Kildishev, "Negative index of refraction in optical metamaterials," *Optics Lett.,* vol. 30, no. 24, pp. 3356–3358, Dec. 2005.
9. J. Zhou, E. N. Economou, T. Koschny C. M. Soukoulis, "Unifying approach to left-handed material design," *Optics Lett*., vol. 31, no. 24, pp. 3620–3622, Dec. 2006.
10. J. Zhou, T. Koschny, L. Zhang, G. Tuttle, and C. M. Soukoulis, "Experimental demonstration of negative index of refraction," *Appl. Phys. Lett.*, vol. 88, p. 221103, 2006.
11. G. Donzelli, A. Vallecchi, F. Capolino, and A. Schuchinsky, "Anisotropic metamaterial made of paired planar conductors: particle resonances, phenomena and properties," *Metamaterials* (Elsevier), vol. 3, no. 1, pp. 10-27, 2009.
12. A. Vallecchi, F. Capolino and A. Schuchinsky, "2-D Isotropic Effective Negative Refractive Index Metamaterial in Planar Technology," *IEEE Microw. Wireless Comp. Lett.,* vol. 19, 2009.
13. F. Yang and Y. Rahmat-Samii, "Reflection phase characterizations of the EBG ground plane for low profile wire antenna applications," *IEEE Trans. Antennas Propagat*., vol.51, no. 10, pp. 2691-2703, Oct. 2003.
14. H. Mosallaei, K. Sarabandi, "Antenna miniaturization and bandwidth enhancement using a reactive impedance substrate," *IEEE Trans. Antennas Propagat*., vol. 52, no .9, pp. 2403-2414, Sep. 2004.